scientific reports

OPEN

The manufacture, optical properties, and mechanical aspects of europium-doped borate glasses

Gharam A. Alharshan[1], A. M. A. Mahmoud[2], Nasra M. Ebrahem[2], Ragab A. Elsad[3✉], Shaaban M. Shaaban[4], Mohamed Elsafi[5] & Shimaa Ali Said[2]

An investigation into the optical and mechanical properties of a novel borate glasses with the chemical composition of $70 B_2O_3$-$10 Li_2O$-$10ZnO$-$5Bi_2O_3$-$5CaO$-xEu_2O_3 was conducted. The glassy specimens of Eu^{3+}-doped borate were prepared by the melting-quenching technique. An enhanced density from 3.0860 to 3.2176 g cm^{-3} and reduced molar volume from 29.27819 to 29.17447 (cm^3 mol^{-1}) are the outcome of increasing the concentration of Eu^{3+} in glasses. Plotting the extinction coefficient, dielectric constant (ε_1, ε_2), and refractive index (n) against wavelength reveals that they all rise as level of Eu^{3+} elements in the glass lattice increases. An increase in Eu^{3+} concentration results in a decrease in both the volume (VELF) and surface (SELF) energy loss functions. Also, all elastic-mechanical moduli (such as Young's, Bulk, Shear, and Elongation) increase with increasing the quantity of Eu^{3+} ions in the glass lattice. The Young's modulus (Y, GPa) of the glassy specimens was 34.512, 36.089, 36.504, 36.730 and 37.114 GPa for x equal 0, 0.25, 0.5, 0.75 and 1 mol ratio in the glass system, and coded by Eu-0.0, Eu-0.25, Eu-0.5, Eu-0.75 and Eu-1.0, respectively. Growing Eu_2O_3 levels resulted in an increase in Micro-Hardness from 2.050 to 2.146 GPa. Poisson's ratio values for Eu-0.0, Eu-0.250, Eu-0.5, Eu-0.75 and Eu-1.0 were 0.273, 0.275, 0.277, 0.277 and 0.278, respectively.

Since long ago, glass, a non-crystalline substance, has been employed in a variety of applications. Furthermore, glasses are significant optical materials that are used extensively in both traditional and contemporary technological advancements due to their linear and nonlinear optical properties. It's important to note that glass's capabilities mostly depend on its ingredients. Glass composition and its fundamental structural component are key factors in determining its characteristics. Additionally, glass composition can be changed to satisfy glass technology requirements. In an attempt to link compositional changes with the evolution of characteristics, many glass systems were developed and investigated[1–4]. Borate glass is regarded as notable among the many oxide glasses because of its unique properties, which include low point of melting, significant RE solubility, good thermal stability, transparency, large refractive index, and affordability[5–8]. Furthermore, because it does not crystallize on its own, it has the highest inclination to create glasses. One of the unique qualities of borate-based compositions is their ability to use the BO_3 and BO_4 structural elements to create a variety of structures[9,10]. Then, new structures can be created by modifying these ones[11,12]. Zinc oxide (ZnO) is added to borate glass to improve the chemical durability of the glass matrix, reduce crystallization, and boost thermal stability[13]. The presence of lithium oxide lowers the glass transition temperature while increasing optical transmission and glass thermal stability[14]. Lithium-based glasses are utilized in modulators, electro-optic switches, and optical parametric devices due to their high conductivity[14]. Bismuth and other heavy metal oxides increase the glass creation range and fluorescence of oxide glasses[15]. Glasses made of bismuth borate have amazing uses in optical devices and non-linear optics. The substantial applications of Bi_2O_3 and ZnO in glasses, such as thermal and mechanical sensors, optical and electrical device layers, infrared transmitting windows, and glass ceramics, have attracted the interest of the scientific community[16].

[1]Physics Department, College of Science, Princess Nourah Bint Abdulrahman University, P.O. Box 84428, 11671 Riyadh, Saudi Arabia. [2]Physics Department, Faculty of Science, AL Azhar University (Girls Branch), Cairo, Egypt. [3]Department of Physics, Faculty of Science, Menoufia University, Shebin El-Koom 32511, Egypt. [4]Department of Electrical Engineering, College of Engineering, Northern Border University, 1321 Arar, Saudi Arabia. [5]Physics Department, Faculty of Science, Alexandria University, Alexandria 21511, Egypt. ✉email: ragab.elsad@gmail.com
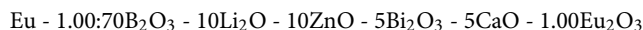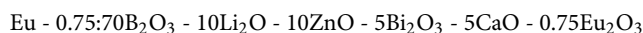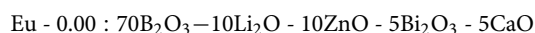
Rare-Earth (RE) ions have the benefit of having f-f transitions that are less affected by ligand field fluctuation. Glasses loaded with RE ions exhibit exceptional emission effectiveness resulting from both 4f-5d and 4f-4f electronic transitions, making them highly efficient luminous materials. Due to its broad emission spectral span, which extends from the blue towards the near-infrared (NIR) location, narrowed emission band, potent emission intensity, beneficial red emission effectiveness, and lengthy excited-state lifespan, europium (Eu³⁺) is considered to be one of the most suitable rare earth ions for injection[17-22].

Glasses doped with Eu³⁺ ions, in particular, have a lot of potential as effective red phosphors and are used in a variety of photonic applications. This is because they have a long radiative lifetime and can emit monochromatic light[23]. The phonon energy of the host material influences the quantum efficiency of rare earth ion emissions. Borate glasses generally have high phonon energy levels because of the network-forming oxides' stretching vibrations. Moreover, in their pure form, it consists of boroxyl BO_3 subunits forming random networks[24]. It is commonly known that the spectroscopic properties of generated (RE) glasses can be improved by the addition of heavier metal oxides, like Bi_2O_3, PbO, CdO, and Sb_2O_3, by lowering the phonon energy, increasing the glass-forming span, and improving the polarizable character of the resulting glass matrix[25-28].

In this work, we have effectively synthesized a variety of new glasses doped with europium oxide that contain lithium, zinc, borate, and heavy metal oxide (bismuth). 70 B_2O_3-10 Li_2O-10ZnO-5Bi_2O_3-5CaO-xEu_2O_3, where x has values of 0.0, 0.25, 0.5, 0.75, and 1.0 (mole ratio), is the formula for the glass compositions. The recently created glasses were then thoroughly characterized to investigate the effects of Eu³⁺ ions on the host glass network structural. This examination included a review of the glasses' mechanical, structural, optical, and physical characteristics.

Experimental

The new glasses used in this study have the following composition: 70 B_2O_3-10 Li_2O-10ZnO-5Bi_2O_3-5CaO-xEu_2O_3, where x (mole ratio) has values of 0.0, 0.25, 0.5, 0.75, and 1.0. Bi_2O_3, B_2O_3, CaO, ZnO, Li_2O, and Eu_2O_3 were all used in extremely pure (99.9%) forms (Aldrich). Twelve grams are produced overall for each composite. The calculated powders are combined in a mortar in a molar ratio for thirty minutes to produce an excellent, homogenous blend. The mixture was melted at a temperature of roughly 1100 °C for 40 min in a porcelain crucible. A homogeneous solution was achieved by physically rotating the porcelain crucible containing the glass sample during the melting process. A brass mold was then used to quench it. Next, in order to remove bubbles and thermal stress from the samples that were created, glasses in a brass mold were placed in a furnace set to 350 °C for 12 h, and the furnace was then allowed to cool to ambient temperature during the annealing process. For the glass samples, the following names are applicable:

$$Eu - 0.00 : 70B_2O_3 - 10Li_2O - 10ZnO - 5Bi_2O_3 - 5CaO$$

$$Eu - 0.25 : 70B_2O_3 - 10Li_2O - 10ZnO - 5Bi_2O_3 - 5CaO - 0.25Eu_2O_3$$

$$Eu - 0.50 : 70B_2O_3 - 10Li_2O - 10ZnO - 5Bi_2O_3 - 5CaO - 0.50Eu_2O_3$$

$$Eu - 0.75 : 70B_2O_3 - 10Li_2O - 10ZnO - 5Bi_2O_3 - 5CaO - 0.75Eu_2O_3$$

$$Eu - 1.00 : 70B_2O_3 - 10Li_2O - 10ZnO - 5Bi_2O_3 - 5CaO - 1.00Eu_2O_3$$

Based on the Archimedes Principle, the density of the generated glass samples was computed using the following formula:

$$\rho_{glass} = \frac{W_{Air}}{(W_{Air} - W_{Liquid})} \times \rho_{Liquid} \tag{1}$$

where W_{Air} and W_{Liquid} represent the sample weight in air and liquid, respectively (the liquid employed was xylene, which has a density of $\rho_{Liquid} = 0.863$ g cm⁻³).

To calculate the molar volume (V_m) of the glass block, the following expression was used:

$$V_m = \frac{glass\ molecular\ weight}{\rho_{glass}} \tag{2}$$

The photograph, density, and estimated molar volume are tabulated in Table 1.

A JASCO UV–Vis-NIR double -beam spectrophotometer model V-570 was used to measure the glasses' optical characteristics.

The Makishima–Mackenzie theory was used in this investigation to compute the elastic mechanical properties of currently produced glass composites[29,30]. The mechanical results depends on the dissociation energy per unit volume (G_t, KJ cm⁻³) and the packing density (V_t, cm³ mol⁻¹) of each composite, which given by $G_t = \sum x_i G_i$ and $V_t = (1/V_m) \sum x_i V_i$, where G_i, V_i and x_i represents the dissociation energy per unit volume, packing factor and molar fraction of iᵗʰ oxide. Through the dissociation energy (G_t) and packing density (V_t) of the studied glass composites estimated by Makishima–Mackenzie's[29,30], the elastic moduli (such as Young (Y), Bulk (B), Shear (S) and Longitudinal (L) modulus) in addition to the Poisson's ratio (δ) as well as the Micro-hardness (H_m) values can be determined from the following relations.

$$Y = 2G_t \cdot V_t \tag{3}$$

Glass code	Sample photo	Density, ρ (g cm⁻³)	Molar volume (cm³ mol⁻¹)	Mechanical characteristics									
				G_t (KJ cm⁻³)	V_i (cm³ mol⁻¹)	V_t (cm³ mol⁻¹)	Y (GPa)	B (GPa)	S (GPa)	L (GPa)	σ	H (GPa)
Eu-0.0		3.0860	29.27819	28.185	17.925	0.612	34.512	25.355	13.554	35.520	0.273	2.050
Eu-0.25		3.1180	29.25988	29.190	18.088	0.618	36.089	26.771	14.149	37.383	0.275	2.119
Eu-0.5		3.1490	29.25123	29.334	18.201	0.622	36.504	27.256	14.295	37.977	0.277	2.127
Eu-0.75		3.1808	29.23538	29.479	18.213	0.623	36.730	27.459	14.381	38.245	0.277	2.137
Eu-1.0		3.2176	29.17447	29.623	18.276	0.626	37.114	27.900	14.517	38.787	0.278	2.146

Table 1. Density, photo, molar volume and mechanical characteristics of the present glass systems.

$$B = 1.2V_t \cdot E \tag{4}$$

$$S = \frac{3YB}{9B - Y} \tag{5}$$

$$L = B + \frac{4}{3}S \tag{6}$$

$$\delta = \frac{Y}{2S - 1} \tag{7}$$

$$H_m = \frac{(1 - 2\delta)Y}{6(1 + \delta)} \tag{8}$$

Compliance with ethical standards
The authors affirm that this manuscript is original, has not been published before, and is not currently being considered for publication elsewhere.

Result and discussion
Density
Table 1 shows that the average density of glasses under assessment increases steadily from 3.0860 towards 3.2176 g cm⁻³ as the Eu level rises from 0.0 to 1.0 mol ratio. Compared to B_2O_3, which is less heavy at 2.46 g cm⁻³, Eu_2O_3 density (7.4 g cm⁻³) is responsible for this increase in density and is essential for the growth of the glass network. An further reason for the greater density of the glasses under investigation is the larger molecular weight of Eu additives (351.926 g mol⁻¹) in comparison to B_2O_3 (69.617 g mol⁻¹). The observed decrease in the molar volume shown in Table 1 could be the result of a reduction in the link length or the interatomic spacing within the glass network, which would create a compact structure within the glass.

Optical properties
The variation of reflectance (R) and transmittance (T) over wavelength (λ) are illustrated in Figs. 1 and 2. Reduced transmittance and increased reflectance are seen. Once the band edge was reached, all of the samples showed high transparency, with the significant transmission range being within 400 and 700 nm throughout the visible region. Transmission measurements (see Fig. 1) show a red shift in the cutoff wavelength, the red shift is mainly attributed to a conversion of three coordination boron atoms $BO_{3/2}$ into $BO_{4/2}$[31]. Eu-0.25 is the sample that yields the greatest transmittance at a rate of almost 70% and smallest reflectance, Eu-0.25 obeys a different trend in the visible region compared to the other samples, higher transmittance of Eu-0.25 indicates higher concentration of BO_4[32], or less absorption by the sample, may due to decrease in the concentration of absorbing molecules. More specifically, Figs. 1 and 2 also show that the reflectance and transmittance spectra for every specimen can
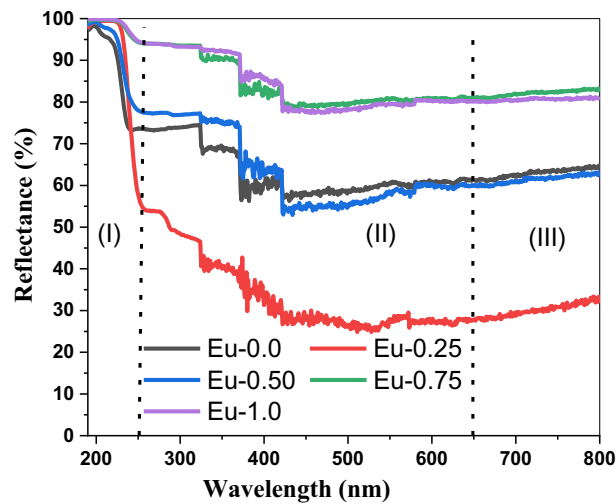
Figure 1. Variation of the reflectance (R) of Eu_2O_3 doped borate glass.
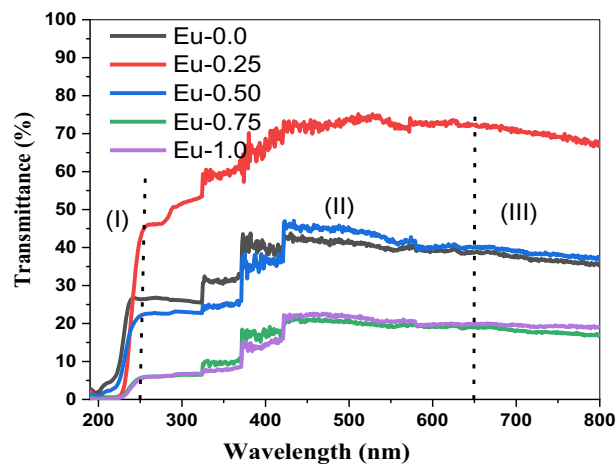

Figure 2. Variation of the Transmittance (T) of Eu_2O_3 doped borate glass.

be categorized into three spectral regions, (I) a strong-absorption locale, where λ is usually shorter than 250 nm, (II) transparent with low reflectance areas where λ usually lies between 250 and 650 nm, (III) no absorption location, which is found at wavelengths beyond 650 nm. In ref.[33], identical behavior was noted.

The fraction of incident light dissipated throughout transmission across the medium can be identified via the extinction coefficient (k), which is calculated as $k = (\alpha\lambda/4\pi)$[34,35]. When electromagnetic waves pass through a substance, the quantity of energy that is absorbed through the material is indicated by the extinction coefficient (k), also known as the absorption index. This indicates that the intensity of the electromagnetic waves will attenuate as they pass along the medium. The proportion of free electrons within the substance and the presence of structural imperfections affect the values of the extinction coefficient (k). Figure 3 displays the variation of (k) with wavelength (λ). We can see from the figure the increasing of (k) levels with increasing Eu_2O_3 concentration. The enhancement in the values of (k) may be assigned to creation the structure defect in the system under consideration by Eu^{3+} content. Absorption intensity of the absorption peaks are increased with Eu_3O_2 content. It can be seen that, most of characteristic absorption bands of Eu_3O_2 ion in the UV and visible region are masked due to strong absorption of the host glass[36,37]. The presence of heavy metal cations such as Bi^{3+} might be responsible for the strong absorption of the glasses. Appearance of absorption peaks in the UV region (200–350 nm) associated with amorphous glass matrix convoyed to chemicals used in preparing glasses. Dufy[38] attributed strong UV absorbance in glasses to the presence of some transition metal ions, e.g. Cr^{6+} and Fe^{3+}, because of the possible charge electron transfer mechanism, even the traces of impurities are in ppm level. It is suggested that the production of superior optical glasses requires the use of exceptionally pure chemicals since they have the potential to impart a strong absorption and the presence of iron ion traces as impurities lower the optical glasses' transmittance[39].
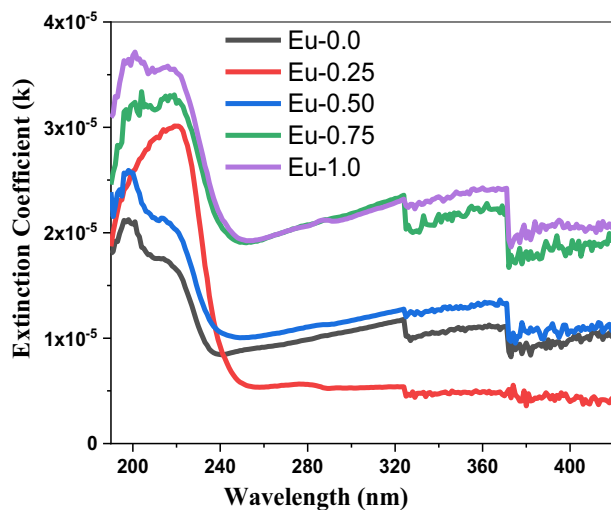
Figure 3. The fluctuation of (k) with wavelength (λ) of Eu_2O_3 doped borate glass.

The following equation can be used to estimate the variation of the refractive index (n) of the present Eu^{3+} ion-doped glass specimens based on absolute value of reflectance (R) as well as extinction coefficient (k)[35,40–42]:

$$n = \frac{(1 + R)}{(1 - R)} + \left(\frac{4R}{(1 - R)^2} - k^2 \right)^{1/2} \tag{9}$$

Figure 4 shows the numerical values of (n) with wavelength λ (nm). It was found that the inclusion of Eu^{3+} ions into the glass structures increased the n levels. The refractive index peak in Fig. 4 increases from sample Eu-0.0 until Eu-1.0 sample, the rise in refractive index indicates a higher optical density for the material.

The dependence of real part of dielectric constant ε_1 on wavelength is shown in Fig. 5, which can be calculated using the following relation[35,40]:

$$\varepsilon_1 = n^2 - k^2 \tag{10}$$

we notice from Fig. 5 that, the effect of the increasing of Eu^{3+} content appears only at lower wavelength or higher energy, also the increase of real part of dielectric constant ε_1 with the variations of the mole ratio of Eu^{3+} ions agreement with the increase of the refractive index level (n).

The imaginary part (ε_2) of dielectric constant was calculated using the equation that follows[35,40]:

$$\varepsilon_2 = 2nk \tag{11}$$

Figure 6 shows the spectrum dependence of ε_2 on wavelength λ (nm) across all doped glass borate samples. The value of both ε_1 and ε_2 were boosted with increase of Eu^{3+} concentration.
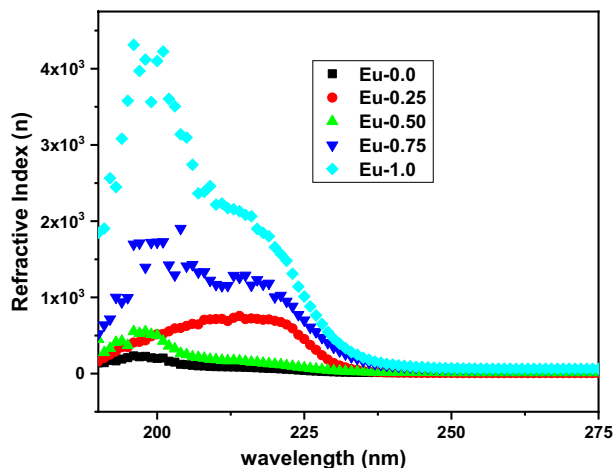

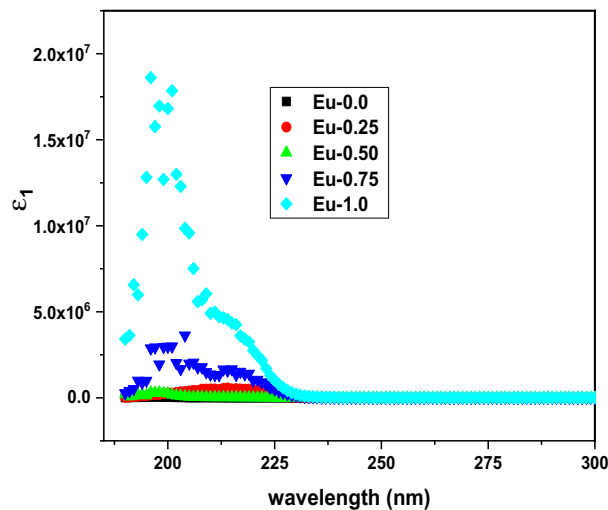**Figure 4.** The values of (n) as a function of with wavelength (λ) of Eu_2O_3 doped borate glass.

Figure 5. The variations of (ε_1) as a function of wavelength (λ) of Eu_2O_3 doped borate glass system.
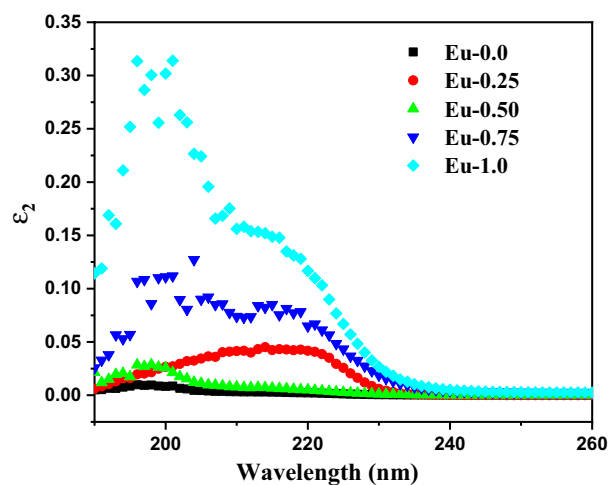

Figure 6. The variations of (ε_2) as a function of wavelength (λ) of Eu_2O_3 doped borate glass system.

Two other important features that can be employed to identify the transitions in optical properties for electrons in this studied are the surface energy loss function (SELF) and the volume energy loss function (VELF). Both factors were utilized to calculate the energy loss rate of electrons during travelling through glass. Via the dielectric function, the energy dissipation is connected to the material's optical characteristics. The probability that the fast electrons will lose power as they go through the bulk and surface of the material is represented by the volume and surface energy loss functions, respectively. The electron transitions within this substance at low and high energies are described by the value of SELF/VELF. VELF and SELF, the two parameters, are provided by equations[40–45]:

$$VELF = \frac{\varepsilon_2}{\left(\varepsilon_1^2 + \varepsilon_2^2\right)} \tag{12}$$

$$SELF = \frac{\varepsilon_2}{\left((\varepsilon_1 + 1)^2 + \varepsilon_2^2\right)} \tag{13}$$

The volume energy loss function (VELF) of the doped borate glass samples with different quantities of Eu_2O_3 was illustrated as a function of wavelength as shown in Fig. 7. As can be observed from that figure, a change in the quantity of Eu_2O_3 causes a change in the electron transition energy, which in turn causes variation in the volume energy loss. Also, the Surface energy loss function is varied due to the variation in Eu^{3+} content as shown in Fig. 8. The values of SELF/VELF as functions of wavelength are plotted in Fig. 9. It is evident that, at the incident wavelength, the volume energy loss was larger than the surface energy loss.
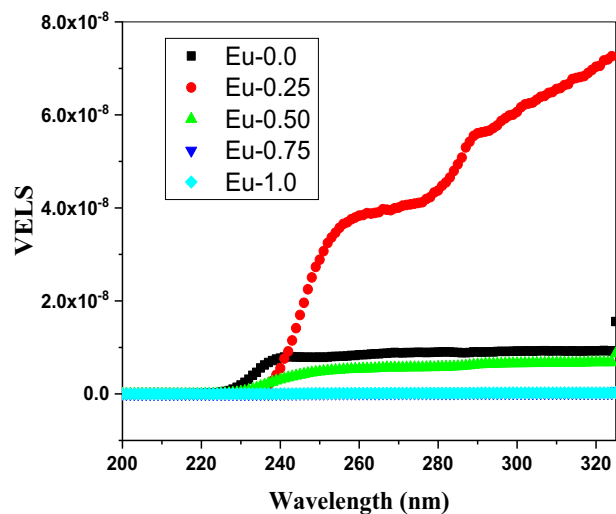
Figure 7. The variations of (VELF) as a function of wavelength (λ) of Eu_2O_3 doped borate glass system.
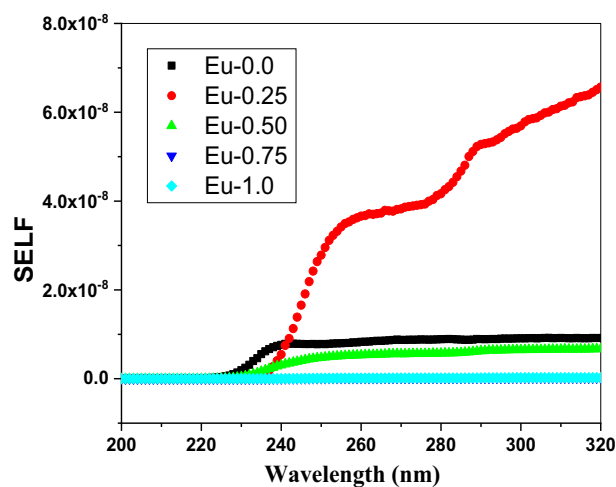

Figure 8. The variations of (SELF) as a function of wavelength (λ) of Eu_2O_3 doped borate glass system.
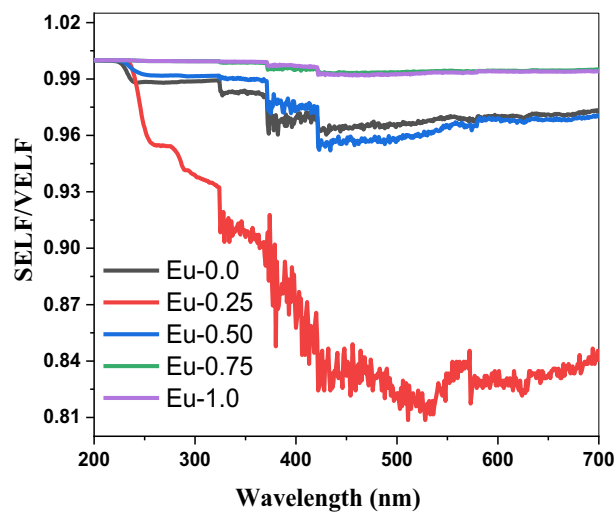

Figure 9. The variations of (VELF/SELF) as a function of wavelength (λ) of Eu_2O_3 doped borate glass system.

Mechanical characteristics

The dissociation energy and packing density were calculated and plotted in Fig. 10. The figure shows an increase in the two factors with the addition of Eu_2O_3 concentration from 0 to 1 mol ratio. The dissociation energy increased from 28.185 to 29.623 kJ cm^{-3}, while the packing density increased from 0.612 to 0.626 cm^3 mol^{-1} as shown in Table 1.

The Young's modulus (Y, GPs) was estimated by the formula in section "Experimental" which measures the rigidity of the fabricated glass. The moduli elasticity results were shown in Fig. 11. The Young's modulus values increased from 34.512 to 37.114 GPs with raising the Eu_2O_3 additives from 0 to 1 mol ratio in the glass system. Due to the addition Eu_2O_3 rare earth to the glass composites, the dissociation energy, or Gibbs-free energy increased which lead to increasing the young's modulus. The other elastic moduli such as Bulk modulus, Shear modulus and longitudinal modulus related to the young modulus are estimated and tabulated in Table 1, and Fig. 11. The longitudinal modulus was greater than the shear and bulk modulus. Poisson's ratio (σ) as well as the microhardness (H, GPa) of the prepared glass composites were calculated based on the results of the elastic modulus, and these parameters measure the extent of expansion/contraction and hardness of the manufactured glass, respectively. The values of Poisson's ratio were 0.273, 0.275, 0.277, 0.277 and 0.278 for Eu-0.0, Eu-0.250, Eu-0.5, Eu-0.75 and Eu-1.0, respectively as shown in Fig. 12, which indicated that Poisson's ratio is approximately relatively constant with Eu_2O_3 additions. Also, the Micro-Hardness was estimated and plotted in Fig. 12, the results increased from 2.050 to 2.146 GPa which showed that the hardness was raised with increasing Eu_2O_3 contents.

The mechanical results depend on the structure of glass composites with changing the doping Eu_2O_3. The FTIR spectra of the borate glasses without Eu_2O_3 and doped with 0.75, and 1.0 mol ratio of Eu_2O_3 is illustrated in Fig. 13 over the spectral range 400–2000 cm^{-1}. From these peaks, three zones can be identified. The first region, spanning 600–700 cm^{-1}, is caused by a B—O—B bending vibration bond in the borate network. The tetrahedral BO_4 units' B—O linkage stretching vibration is responsible for the second region, which spans from 800 to 1200 cm^{-1}, and the triangles-BO_3 units' B—O stretching vibration is responsible for the third zone, which spans from 1200 to 1600 cm^{-1}[46–48]. More information regarding structural alterations was found by using FTIR deconvolution techniques shown in Fig. 14. Several peaks were seen in the infrared spectra of the glasses at 673, 882, 1048, 1239, 1405, and 1754 cm^{-1}. The bending vibrations of bridging oxygen (B—O) over trigonal BO_3 groups are suggested to be the origin of a band at 673 cm^{-1}[49]. The band at 882 cm^{-1} further confirms connectivity between the diporate and B-O-B networks. Furthermore, the bands at 1239 cm^{-1} were shown to be caused by the asymmetric stretching of the B–O connection in BO_3 units made from boroxels. The symmetric stretching relaxation of the B—O band, caused by the trigonal BO_3 units, is responsible for the peak at around 1405 cm^{-1}[50]. The two other peaks, measured at 1572 and 1969 cm^{-1}, are the result of B—O stretching vibrations, or BO_3 units, in triangles[46–48].

The change in the relative areas of peak absorption linked to BO_4 and BO_3 groups, N_4 and N_3, respectively, is one of the most significant finds. N_4 and N_3 can be calculated using the relations listed below.

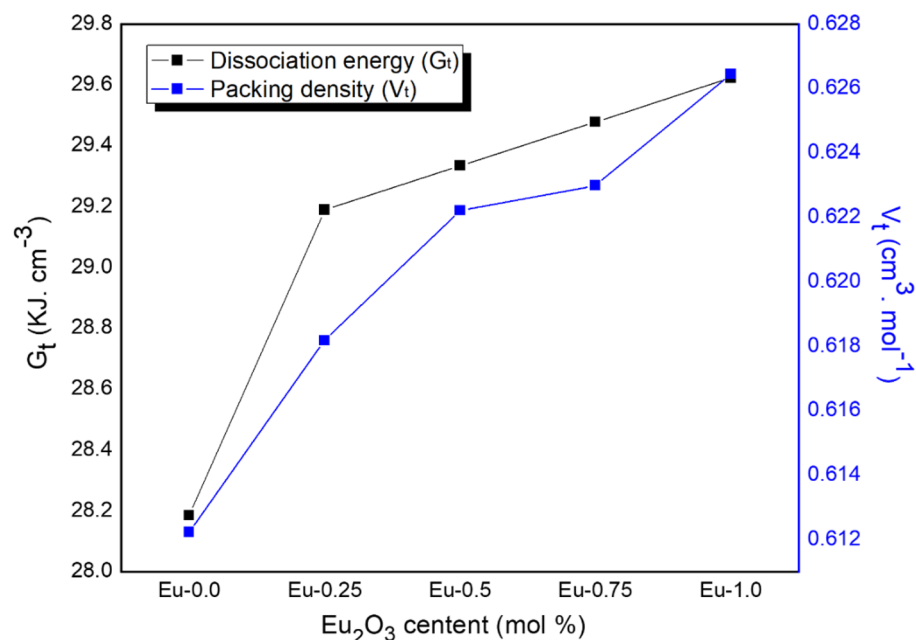$$N4 = \frac{A4}{A4 + A3}, \quad N3 = \frac{A3}{A4 + A3} \tag{14}$$

Figure 10. The variation of dissociation energy and packing density of Eu-glass composites.
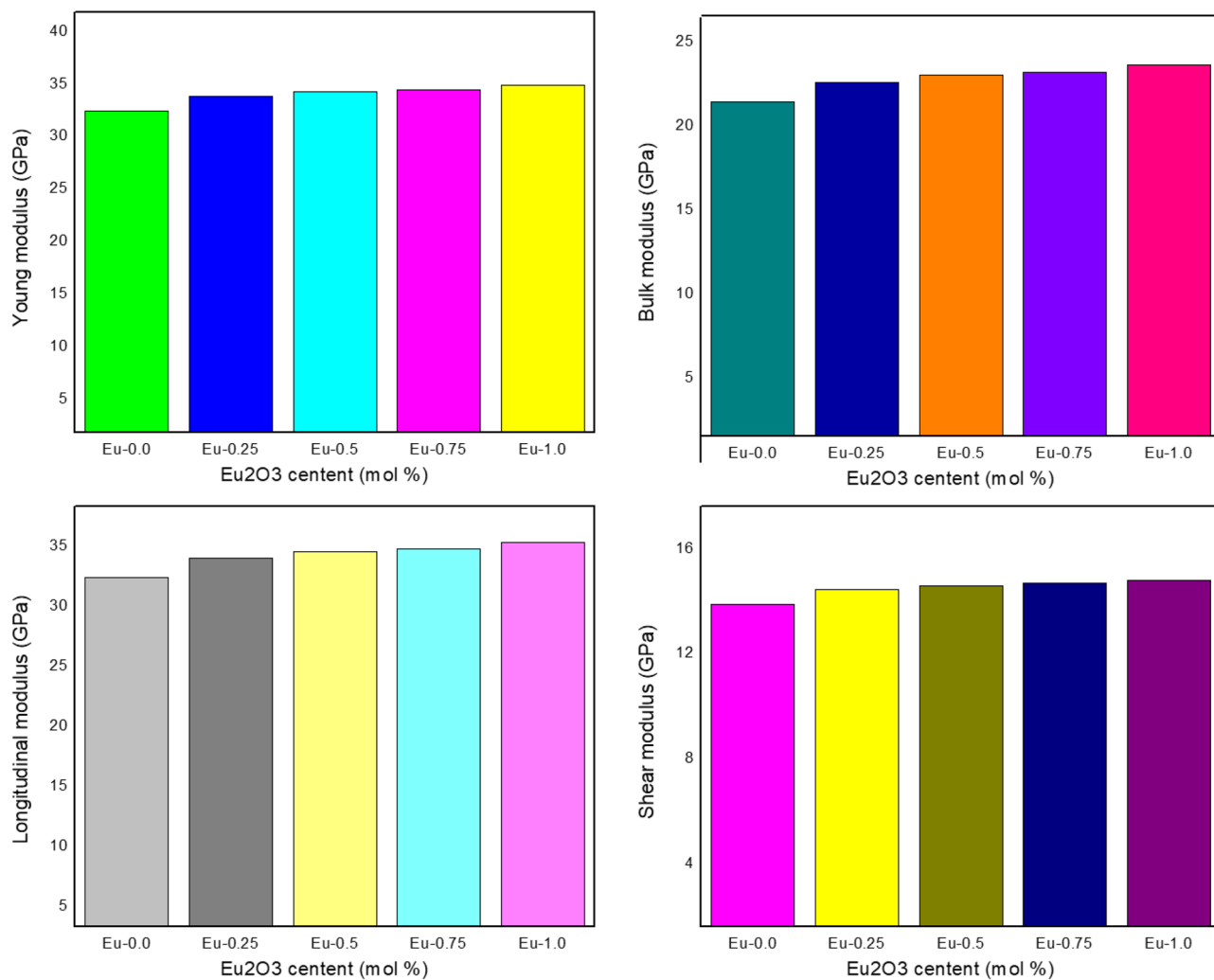
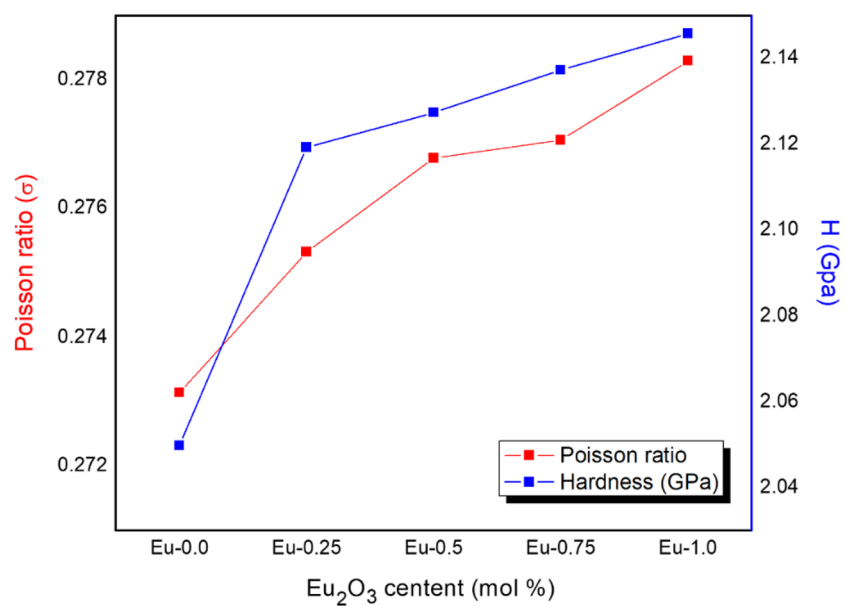**Figure 11.** The variation of Young, shear, Longitudinal and Bulk modulus of Eu-glass composites.

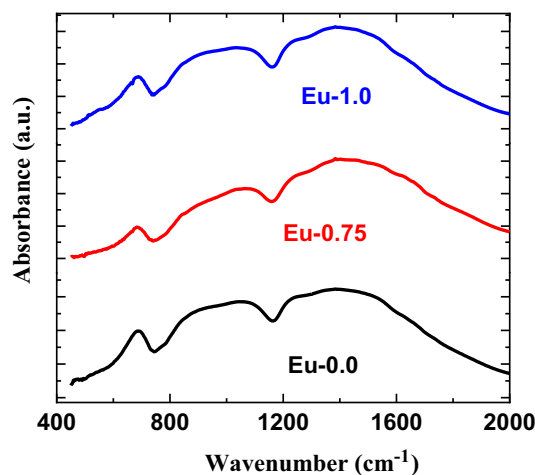**Figure 12.** The variation of Poisson ratio and micro-hardness of Eu-glass composites.

Figure 13. FTIR spectra of the borate glasses without Eu_2O_3 and doped with 0.75, and 1.0 mol ratio of Eu_2O_3.
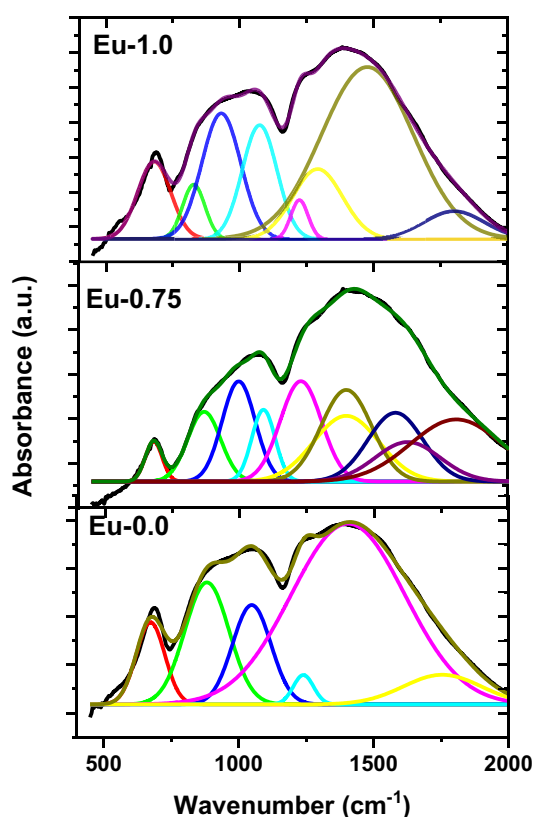

Figure 14. FTIR deconvolution of the borate glasses without Eu_2O_3 and doped with 0.75, and 1.0 mol ratio of Eu_2O_3.

In the present case, the regions under the BO_3 and BO_4 group's absorption peaks of Eu-0.0, Eu-0.75, and Eu-1.0 are equal 0.653, 0.634, 0.632 and 0.347, 0.366, 0.368, respectively. As clear, the relative value of BO_4 rises with lowering BO_3 values that cause improving the compatibility and stiffness for the doped samples. Increments in BO_4 result in increasing not only the density but also the connectivity and the stiffness and elasticity of the glass system. It is clear that the structure with doping Eu_2O_3 increase the mechanical properties of present glass.

Finally, the mechanical results of this study were compared with related published values for $BaO-PbO-P_2O_5$ glass system[51]. The comparison showed a superiority in the mechanical properties of the manufactured glass samples compared to BaO-PbO-P2O5 system, as the maximum young modulus in the published sample BPP7 (50 BaO + 50 P2O5) was 36.655 GPa, while the maximum value in the present results was 37.114 GPs. The current young modulus results also compared with the $Bi_2O_3–PbO–CdO–B_2O_3$[52], the sample with the highest density

consists of $25Bi_2O_3–30PbO–10CdO–35B_2O_3$, and its young's modulus was 35.07 GPa, while the bulk modulus was 19.97 GPa. These values are lower than the values for the present glass composites studied in the current work, which indicates that they provide good mechanical results and can be used in different applications.

Conclusions

A study was carried out to examine the optical and mechanical characteristics of a new borate glass system that contains $70 B_2O_3$-10 Li_2O-10ZnO-5Bi_2O_3-5CaO-xEu_2O_3 that were made using the melting-quenching method. The result of raising the Eu^{3+} concentration in glasses is an improved density. The glass structure exhibits an increase in dielectric constant (ε_1, ε_2), extinction coefficient, reflectance, and refractive index as the quantity of Eu^{3+} ions increases. The spectrum transmittance and both surface and volume energy loss function (SELF and VELF) are decrease with increasing Eu^{3+} ions. The result of raising the Eu^{3+} concentration in fabricated glass led to improve the mechanical properties. The young's modulus, shear modulus, bulk modulus and micro- Hardness are increases with increasing Eu^{3+} ions in the glass structure, this is due to the raising the dissociation energy in the glass composite increased with increasing the Eu^{3+} concentration.

Data availability

All data generated or analyzed during this study are included in this published article.

References

1. Ahmmad, S. K. *et al.* Machine learning density prediction and optical properties of calcium boro-zinc glasses. *Opt. Mater.* **134**, 113145 (2022).
2. Alsaif, N. A. *et al.* Antimony (III) oxide-reinforced lithium-calcium borate glasses: Preparation and characterization of physical, optical, and γ-ray shielding behavior through experimental and theoretical methods. *J. Mater. Sci.: Mater. Electron.* **51**, 5869–5879 (2022).
3. Alsaif, N. A. M., Khattari, Z. Y., Rammah, Y. S., Shams, M. S. & Elsad, R. A. Bismo-borate glasses doped with La^{3+} and Eu^{3+} ions: Synthesis, physical, optical and electrical characteristics. *J. Mater. Sci.: Mater. Electron.* **33**, 19667–19677 (2022).
4. Rammah, Y. S. *et al.* Synthesis, physical, FTIR, and optical characteristics of B_2O_3·CaO·ZnO glasses doped with Nb_2O_5 oxide: Experimental investigation. *J. Mater. Sci. Mater.* **33**, 23749–23760 (2022).
5. Kavaz, E. An experimental study on gamma-ray shielding features of lithium borate glasses doped with dolomite, hematite and goethite minerals. *Radiat. Phys. Chem.* **160**, 112–123. https://doi.org/10.1016/j.radphyschem.2019.03.032 (2019).
6. Alsaif, N. A. M. *et al.* Synthesis, structure, radiation attenuation efficacy as well as prediction of density using artificial intelligence techniques of lead borate lithium zinc strontium glasses. *Opt. Mater.* **137**, 113599 (2023).
7. Shaaban, S. M. *et al.* Influence of copper ions on the structural, mechanical, radiation shielding and dielectric properties of borate zinc-fluoride glasses. *J. Electron. Mater.* **52**, 6269–6276 (2023).
8. Abdel-Aziz, A. M. *et al.* Synthesis, physical, ultrasonic waves, mechanical, FTIR, and dielectric characteristics of B_2O_3/Li_2O/ZnO glasses doped with Y^{3+} ions. *J. Mater. Sci. Mater. Electron.* **33**, 6603–6615 (2022).
9. Deopa, N. & Rao, A. S. Spectroscopic studies of Sm^{3+} ions activated lithium lead alumino-borate glasses for visible luminescent device applications. *Opt. Mater.* **72**, 31–39 (2017).
10. Maheshvaran, K., Veeran, P. K. & Marimuthu, K. Structural and optical studies on Eu^{3+} doped boro-tellurite glasses. *Solid State Sci.* **17**, 54–62 (2013).
11. Khalil, E. M. A. *et al.* UV-visible and IR spectroscopic studies of gamma irradiated transition metal doped lead silicate glasses. *Silicon* **2**(1), 49 (2010).
12. Abdelghany, A. M., Abdelrazek, E. M., Badr, S. I., Abdel-Aziz, M. S. & Morsi, M. A. Efect of Gamma-irradiation on biosynthesized gold nanoparticles using Chenopodiummurale leaf extract. *J. Saudi Chem. Soc.* **21**(5), 528 (2017).
13. Ahlawat, J. *et al.* Structural and optical characterization of IR transparent sodium-modified zinc borate oxide glasses. *Appl. Phys. A* **128**, 923 (2022).
14. Pawaria, S. *et al.* Structural and optical characterization of semiconducting lithium modified zinc borate glassy system for UV band reject filter. *J. Mol. Struct.* **1270**, 133836 (2022).
15. Narwal, P. *et al.* Improved white light emission in Dy^{3+} doped LiF – CaO – Bi_2O_3 – B_2O_3 glasses. *J. Non Cryst. Solids* **498**, 470–479. https://doi.org/10.1016/j.jnoncrysol.2018.01.042 (2018).
16. Bala, M. *et al.* Effect of replacement of Bi_2O_3 by Li_2O on structural, thermal, optical and other physical properties of zinc borate glasses. *J. Mol. Struct.* **1219**, 128589 (2020).
17. Bouabdalli, E. M., El Jouad, M., Hajjaji, A., Garmim, T. & Touhtouh, S. Synthesis and characterization of silicophosphate glasses doped with europium. *Mater. Today: Proc.* https://doi.org/10.1016/J.MATPR.2022.04.299 (2022).
18. Anjaiah, J., Laxmikanth, C. & Veeraiah, N. Spectroscopic properties and luminescence behavior of europium doped lithium borate glasses. *Phys. B Condens. Matter* **454**, 148–156. https://doi.org/10.1016/j.physb.2014.07.070 (2014).
19. Selvi, S., Marimuthu, K. & Muralidharan, G. Structural and luminescence studies of Eu^{3+}: TeO_2[sbnd]B_2O_3[sbnd]AO[sbnd]AF_2 (A = Pb, Ba, Zn, Cd, Sr) glasses. *J. Mol. Struct.* **1144**, 290–299. https://doi.org/10.1016/j.molstruc.2017.05.031 (2017).
20. Selvi, S., Marimuthu, K., Suriya-Murthy, N. & Muralidharan, G. Red light generation through the lead boro-telluro-phosphate glasses activated by Eu^{3+} ions. *J. Mol. Struct.* **1119**, 276–285. https://doi.org/10.1016/j.molstruc.2016.04.073 (2016).
21. Sajna, M. S. *et al.* Spectroscopic investigations and phonon side band analysis of Eu^{3+}-doped multicomponent tellurite glasses. *Opt. Mater. Amst.* **70**, 31–40. https://doi.org/10.1016/j.optmat.2017.04.064 (2017).
22. El-Jouad, M. *et al.* Red luminescence and UV light generation of europium doped zinc oxide thin films for optoelectronic applications. *EPJ Appl. Phys.* **2020**, 91. https://doi.org/10.1051/epjap/2020200133 (2020).
23. Malchukova, E., Boizot, B., Ghaleb, D. & Petite, G. Optical properties of pristine and γ-irradiated Sm doped borosilicate glasses. *Nucl. Instrum. Methods Phys. Res.* **537**, 411–414. https://doi.org/10.1016/j.nima.2004.08.054 (2005).
24. Hatefi, Y., Shahtahmasebi, N., Moghimi, A. & Attaran, E. Frequency-conversion properties of Eu^{3+} doped chlorophosphate glass ceramics containing $CaCl_2$ nanocrystals. *J. Lumin.* **131**, 114–118. https://doi.org/10.1016/j.jlumin.2010.09.029 (2010).
25. Doerenkamp, C. *et al.* Composition–structure–property correlations in rare-earth-doped heavy metal oxyfluoride glasses. *J. Phys. Chem. C* **123**(36), 22478–22490. https://doi.org/10.1021/acs.jpcc.9b05531 (2019).
26. Ouannes, K. *et al.* New Er^{3+} doped antimony oxide based glasses: Thermal analysis, structural and spectral properties. *J. Alloys Compd.* **649**, 564–572. https://doi.org/10.1016/j.jallcom.2015.07.113 (2015).

27. Marzouk, M. A., Ouis, M. A. & Hamdy, Y. M. Spectroscopic studies and luminescence spectra of Dy_2O_3 doped lead phosphate glasses. *Silicon* **4**(3), 221–227. https://doi.org/10.1007/s12633-012-9125-z (2012).
28. ElBatal, F. H., Marzouk, M. A. & Abdel-Ghany, A. M. Gamma rays interaction with bismuth borate glasses doped by transition metal ions. *J. Mater. Sci.* **46**, 5140–5152. https://doi.org/10.1007/s10853-011-5445-4 (2011).
29. Makishima, A. & Mackenzie, J. D. Direct calculation of Young's modulus of glass. *J. Non-Cryst. Solids* **12**, 35–45 (1973).
30. Makishima, A. & Mackenzie, J. D. Calculation of Bulks modulus, Shear modulus and Piosson's ratio of glass. *J. Non-Cryst. Solids* **17**, 147–157 (1975).
31. El-Diasty, F., Moustafa, F. A., Abdel-Wahab, F. A., Abdel-Baki, M. & Fayad, A. M. Role of 4p–3d orbital hybridization on band gap engineering of heavy metal glass for optoelectronic applications. *J. Alloys Compd.* **605**, 157–136 (2014).
32. Colak, S. C. & Kilic, G. Structural, physical, and optical characterization of (Nd^{3+}/Eu^{3+})-doped zinc-rich silica–borate glasses. *J. Mater. Sci.: Mater. Electron.* **33**, 21852–21863 (2022).
33. Hassanien, A. S. & Akl, A. A. Optical characteristics of iron oxide thin films prepared by spray pyrolysis technique at different substrate temperatures. *Appl. Phys. A* **124**, 752. https://doi.org/10.1007/s00339-018-2180-6 (2018).
34. Hodgson, J. N. *Optical Absorption and Dispersion in Solids* (Springer, New York, 2012). https://doi.org/10.1007/978-1-4613-3321-0.
35. Mahmoud, W. E., Shirbeeny, W., Al-Ghamdi, A. A. & Al-Heniti, S. Synthesis and characterization of $Cd_xZn_{1-x}O$ nanoparticles-doped aryl poly ether ketone for novel application potentials. *J. Appl. Poly. Sci.* **125**, 339. https://doi.org/10.1002/app.35570 (2012).
36. Jamalaiah, B. C., Moorthy, L. R., Seo, H. J. & Non-Cryst, J. Effect of lead oxide on optical properties of Dy3+ ions in PbO–H3BO3–TiO2–AlF3 glasses. *Solids* **358**, 204–209 (2012).
37. Ramesh, P., Hegde, V., Pramod, A. G., Eraiah, B. & Agarkov, D. A. Compositional dependence of red photoluminescence of Eu_3O_2 ions in lead and bismuth containing borate glasses. *Solid State Sci.* **107**, 106360 (2020).
38. Dufy, J. A. Charge transfer spectra of metal ions in glass. *Phys. Chem. Glasses* **38**, 289–292 (1997).
39. Hussein, E. M. A. & Rammah, Y. S. Optical UV–visible, Raman spectroscopy, and gamma radiation shielding properties of borate glass systems; $B_2O_3+Na_2O+Al_2O_3/MgO/Li_2O$. *Opt. Quant. Electron.* **56**, 387 (2024).
40. Taha, T. A. & Rammah, Y. S. Optical characterization of new borate glass doped with titanium oxide. *J. Mater. Sci. Mater. Electron.* **27**(2), 1384–1390. https://doi.org/10.1007/s10854-015-3901-7 (2016).
41. Taha, T. A. & Abouhaswa, A. S. Preparation and optical properties of borate glass doped with MnO2. *J. Mater. Sci.: Mater. Electron.* **29**, 8100–8106 (2018).
42. Hodgson, J. N. *Optical Absorption and Dispersion in Solids* (Springer, 2012).
43. Ebnalwaled, A. A., Sadek, A. H., Ismail, S. H. & Mohamed, G. G. Structural, optical, dielectric and surface properties of polyimide hybrid nanocomposites films embedded mesoporous silica nanoparticles synthesized from rice husk ash for optoelectronic applications. *Opt. Quant. Electron.* **54**, 690. https://doi.org/10.1007/s11082-022-03976-2 (2022).
44. Sarkar, S., Das, N. S. & Chattopadhyay, K. K. Optical constants, dispersion energy parameters and dielectric properties of ultra-smooth nanocrystalline $BiVO_4$ thin films prepared by rf-magnetron sputtering. *Solid State Sci.* **33**, 58–66. https://doi.org/10.1016/j.solidstatesciences.2014.04.008 (2014).
45. Ali, A. I., Son, J. Y., Ammar, A. H., Moez, A. A. & Kim, Y. S. Optical and dielectric results of Y0.225Sr0.775CoO3±δ thin films studied by spectroscopic ellipsometry technique. *Results Phys.* **3**, 167–172. https://doi.org/10.1016/j.rinp.2013.08.004 (2013).
46. Gupta, N. *et al.* Structure-property correlations in TiO_2-Bi_2O_3-B_2O_3-TeO_2 glasses. *J. Non-Cryst. Solids* **470**, 168–177 (2017).
47. Kaky, K. M. *et al.* Stuctural, optical and radiation shielding properties of zinc boro-tellurite alumina glasses. *Appl. Phys. A.* **125**, 32 (2019).
48. Malge, A. *et al.* Structural and DC conductivity studies of borotellurite glasses doped with ZnO, Li_2O and Dy_2O_3. *Mater. Today: Proc.* **26**, 1960–1963 (2020).
49. Es-soufi, H., Bih, H., Sayyed, M. I. & Bih, L. Impact of TiO_2 on physical, optical, and radiation shielding properties of tungsten-based glasses. *Optik* **272**, 170400 (2023).
50. Kaur, R. *et al.* Physical, optical, structural and thermoluminescence behaviour of borosilicate glasses doped with trivalent neodymium ions. *Opt. Mater.* **117**, 111109 (2021).
51. Mahmoud, K. A., El-Agawany, F. I., Tashlykov, O. L., Ahmed, E. M. & Rammah, Y. S. The influence of BaO on the mechanical and gamma/fast neutron shielding properties of lead phosphate glasses. *Nucl. Eng. Technol.* **53**, 3816–3823 (2021).
52. Almuqrin, A. H. *et al.* Mechanical and gamma-ray shielding examinations of Bi2O3–PbO–CdO–B2O3 glass system. *Open Chem.* **20**, 808–815. https://doi.org/10.1515/chem-2022-0195 (2022).

Acknowledgements

Author contributions

G AA, AMM, and ME wrote the main body of the manuscript; RAE, SAS, SMS, and NME created and interpreted all of the figures; all authors revised the work.

Competing interests

The authors declare no competing interests.

Additional information

Correspondence and requests for materials should be addressed to R.A.E.

Reprints and permissions information is available at www.nature.com/reprints.

Publisher's note Springer Nature remains neutral with regard to jurisdictional claims in published maps and institutional affiliations.